Available online at www.sciencedirect.com
ScienceDirect
Journal of Power Sources 173 (2007) 781–787
JOURNAL OF POWER SOURCES
www.elsevier.com/locate/jpowsour

Superionic phase transition in $Rb_3D(SeO_4)_2$ single crystals

Antoni Pawłowski [a,*], Maria Połomska [a], Bożena Hilczer [a], Ludwik Szcześniak [a], Adam Pietraszko [b]

[a] *Institute of Molecular Physics, Polish Academy of Sciences, Poznań, Poland*
[b] *Institute of Low Temperatures and Structure Researches, Polish Academy of Sciences, Wrocław, Poland*

Available online 24 May 2007

Abstract

$Rb_3D(SeO_4)_2$ belongs to the well-known group of hydrogen sulfate and selenate crystals which are promising for fuel cell applications. However, the high temperature properties of this salt have been much less extensively studied than those of $Rb_3H(SeO_4)_2$. Superionic phase transition in $Rb_3D(SeO_4)_2$ and $Rb_3H(SeO_4)_2$ single crystals was studied using impedance spectroscopy and DSC methods. Temperature evolution of the ferroelastic domain structure was observed under a polarizing microscope. Additionally, the X-ray diffraction and Raman scattering measurements for both crystals were carried out at room temperature. $Rb_3D(SeO_4)_2$ undergoes a structural phase transition from the low temperature ferroelastic phase to the superionic, paraelastic one. A correlation was found between the ferroelastic domains evolution, the anomalies of DSC and the temperature dependence of ionic conductivity. The temperature range of superionic phase transition in the first heating run was much wider and the T_S value was lower in $Rb_3D(SeO_4)_2$ than in the non-deuterated compound. Additionally, a considerable temperature hysteresis of T_S in $Rb_3D(SeO_4)_2$ was observed, unlike in $Rb_3H(SeO_4)_2$. The activation energies of H^+ and D^+ conductivity along the *c*-axis were found to be almost the same. The temperature variation of ionic conductivity in $Rb_3D(SeO_4)_2$ obtained in the first heating run of a virgin sample was found to differ considerably from that measured in subsequent cooling/heating runs. The small H/D isotope effect of proton conductivity in the crystals studied pointed to a classical activated diffusion mechanism.

Keywords: Protonic conductor; Trirubidium hydrogen biselenate; Isotope effect; Ferroelasticity; Superprotonic phase transition

1. Introduction

A common feature of hydrogen sulfate and selenate crystals of the general chemical formula $A_xH_y(XO_4)_{(x+y)/2}$, where A denotes Rb, Cs, NH_4, and X is S or Se, is the hydrogen bonding. The structural motif of the crystals consists of XO_4 tetrahedra linked with short hydrogen bonds into isolated dimers (in the group of $x=3$ and $y=1$), into infinite chains (when $x=1$ and $y=1$) and into trimers (for $x=4$ and $y=2$). At the superionic phase transition temperature T_S, ranging from 300 K for $(NH_4)_3H(SeO_4)_2$ to ~490 K for $Rb_3H(SO_4)_2$, the materials undergo a transition to the phase with a fast proton transport. In some compounds the temperature T_S coincides with the ferroelastic–paraelastic phase transition temperature T_C.

Although all the above crystals are water soluble and mechanically "plastic" in the superionic phase, a successful operation of a fuel cell with $CsHSO_4$ ($T_S = 141\,^\circ C$) as a membrane material was reported a few years ago [1]. Acid salt electrolyte-based fuel cell offers several advantages over a polymeric one. The salts are "true" proton conductors, with no water involved in the conduction mechanism, so careful water management in a fuel cell is not necessary. Furthermore they exhibit superprotonic conductivity at elevated temperatures, thus the purity requirements on the hydrogen fuel are relaxed, catalyst activity is increased and waste heat is more easily manageable. At present a major shortcoming of hydrogen sulfate and selenate electrolytes is their catalyzed reduction under hydrogen atmosphere, accompanied by the generation of H_2S, which is an effective catalyst poison [2].

$Rb_3H(SeO_4)_2$ and $Rb_3D(SeO_4)_2$ crystals are ferroelastic, with $C2/c$ space group at room temperature and transform to superprotonic (paraelastic) phase of $R\bar{3}m$ space group at T_S. In the low temperature phase the structural motif consists of isolated dimers formed by asymmetric SeO_4 tetrahedra linked with short H/D bonds between apical O(2) oxygen atoms of neighboring molecules. Protons (deuterons) occupy one of the two potential minima between their respective donor

* Corresponding author. Tel.: +48 61 86 951 44; fax: +48 61 86 845 24.
E-mail address: antoni@ifmpan.poznan.pl (A. Pawłowski).

0378-7753/$ – see front matter © 2007 Elsevier B.V. All rights reserved.
doi:10.1016/j.jpowsour.2007.05.068

and acceptor, so the bonds are ordered (i.e. their direction in the lattice does not change). The pattern is referred to as the so-called zero-dimensional hydrogen-bond network. The O(2) atoms and therefore the H-bonds form layers parallel to the (0 0 1) plane [3]. In this phase the number of structurally equivalent positions for protons equals their number, so any proton conductivity has to involve defect sites. As a result, the conductivity is low and its activation energy value high.

Above T_S, in the trigonal symmetry phase, two additional directions of hydrogen bonds in the (0 0 1) plane are symmetry equivalent. The directions differ by $+2\pi/3$ and $-2\pi/3$ from that in the monoclinic phase. In this way the number of structurally equivalent positions for protons (deuterons) increases three times [3]. The proton transport proceeds via structure diffusion (Grotthus mechanism) and consists of two steps: (1) proton transfer in an H-bond, from donor to acceptor and (2) reorientation of the $HSeO_4$ group (which involves breaking of the H-bond) to a position at which a new bond can be formed. It means that a proton encounters two energy barriers along its conduction path: the one separating the energy minima for transfer from donor to acceptor and the barrier for the $HSeO_4$ group reorientation.

The fast proton transport in the crystals is conditioned by molecular dynamics of the proton environment which involves both vibrational and librational modes of the SeO_4 tetrahedra and lowers the two barriers for proton transport [4]. As a result, each proton forms H-bonds with three O(2) oxygen atoms of the nearest SeO_4 groups with the same probability $p = 1/3$. In this way protons (and consequently H-bonds) are de-localized in the superionic phase and form a dynamically disordered network of H-bonds in the (0 0 1) plane [5,6]. The arrangement of H-bonds in layers results in a distinct anisotropy of proton conductivity, which is ~20 times higher in the plane than along the direction perpendicular to it [7].

At low temperatures a dramatic H/D isotope effect in the title compound was reported. $Rb_3D(SeO_4)_2$ undergoes antiferroelectric phase transition at 92 K, whereas the protonated crystal does not exhibit any transition below room temperature [8,11,12]. On the other hand, insignificant isotope effect on the superionic transition was observed in other acid salt $CsHSO_4$: T_S in $CsDSO_4$ was by ~2 K lower and the activation energy of deuteron transport by 0.01–0.02 eV higher than in $CsHSO_4$, whereas the effect on the ionic conductivity was expressed by $\sigma^H/\sigma^D = 2.3$ and ~1.5 [13,14]. Considering a much pronounced isotope effect in $Rb_3H(SeO_4)_2$ at low temperatures, it seems interesting to study the isotope exchange influence on the superionic phase transition in this crystal.

Impedance spectroscopy conductivity measurements of $Rb_3H(SeO_4)_2$ have shown that the temperature T_S ranges from 449 K to 456 K [3,8,9] and the activation energy in the high conducting phase is $E_a = E_b \approx 0.28$ eV, $E_c \approx 0.48$ eV along the *a*, *b*, and *c* crystallographic axes, respectively [7]. For $Rb_3D(SeO_4)_2$, the values of $T_S = 460$ K and $E_c = 0.28$ eV in the superionic phase were obtained from the conductivity measurements at 100 kHz [10].

2. Experimental

$Rb_3D(SeO_4)_2$ was obtained by 6-fold recrystallization from D_2O. Single crystals of pseudo-hexagonal habit were grown from stoichiometric D_2O solution of the deuterated salt by slow evaporation at room temperature. The degree of deuteration was controlled by NMR and amounted to ~90%. $Rb_3H(SeO_4)_2$ crystals were grown by slow evaporation at room temperature from aqueous solution of the salt. Differential scanning calorimetry (DSC) studies were performed with Netzsch DSC-200 calorimeter at a heating/cooling rate of 2 K min^{-1}.

The temperature evolution of the ferroelastic domain pattern was studied in the (0 0 1) plane using a polarizing optical microscope equipped with a LINKAM cooling–heating stage. The temperature was changed at a rate of 0.5 K min^{-1}.

The ionic conductivity along the *c*-axis, σ_c, of both crystals was measured in air by the impedance spectroscopy method with a computer controlled HP-4192A Impedance Analyzer. The measuring voltage was 0.5 V, in 100–10 MHz frequency range. For conductivity measurements samples of ~10 mm^2 in area and ~0.4 mm thick were used. The electrodes were made by covering the opposite (0 0 1) faces with silver paste. Each complex impedance plot was obtained at a temperature stabilized to within 0.03 K.

NIR Raman spectra ($\lambda = 1064$ nm) were recorded at room temperature with a BRUKER IFS66 FRA106 spectrometer in the 180° geometry. Integrated X-ray intensities were collected on an Xcalibur (Oxford Diffraction Company) diffractometer equipped with a CCD detector, using graphite monochromated Mo Kα radiation. Unshaped crystals of 0.23 mm ($Rb_3D(SeO_4)_2$) and 0.26 mm ($Rb_3H(SeO_4)_2$) in average diameter were used. The measurements were carried out at 15 K and 295 K for $Rb_3D(SeO_4)_2$ and 120 K and 295 K for $Rb_3H(SeO_4)_2$. Low temperature was maintained with a HeliJet gas-flow cooling system (Oxford Diffraction Controller), $\Delta T = 0.3$ K. The CrysAlis software version 1.170.2 (Oxford Diffraction) was used for the data processing. The crystal structure of both salts was determined and refined at all temperature points using the SHELXL-97 program package.

3. Results

3.1. DSC study

DSC measurements (Fig. 1) show that the superionic phase transition in $Rb_3D(SeO_4)_2$ is stretched over ~18 K and is completed at ~451 K on the first heating, whereas on cooling it is finished at ~430 K. The transition enthalpy $\Delta H \approx 3.4$ kJ $mole^{-1}$. It should be added that the temperature of the DSC maximum on heating is close to the temperature at which new twin walls start to appear on the domain structure observations.

DSC spectra of $Rb_3H(SeO_4)_2$ are shown in Fig. 2. The superionic phase transition is stretched over 6–8 K and the transition enthalpy $\Delta H \approx 3.8$ kJ $mole^{-1}$. The transition is completed at ~460 K on heating and at ~450 K on cooling.

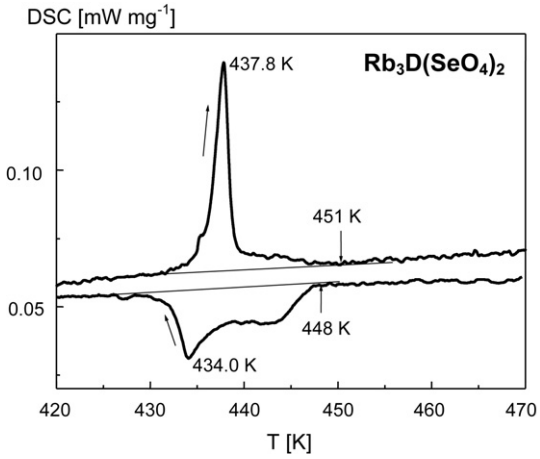

Fig. 1. DSC scans for $Rb_3D(SeO_4)_2$ obtained in the first heating/cooling cycle.

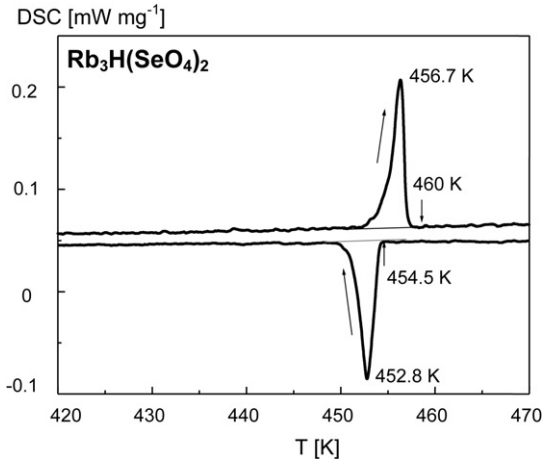

Fig. 2. DSC scans for $Rb_3H(SeO_4)_2$ obtained in the first heating/cooling cycle.

3.2. Impedance spectroscopy study of $H^+(D^+)$ conductivity

Proton conductivity studies have also revealed differences in the behavior of $Rb_3H(SeO_4)_2$ crystal and its deuterated analogue (Fig. 3). The $\sigma_c(1/T)$ dependence, obtained in the first heating run

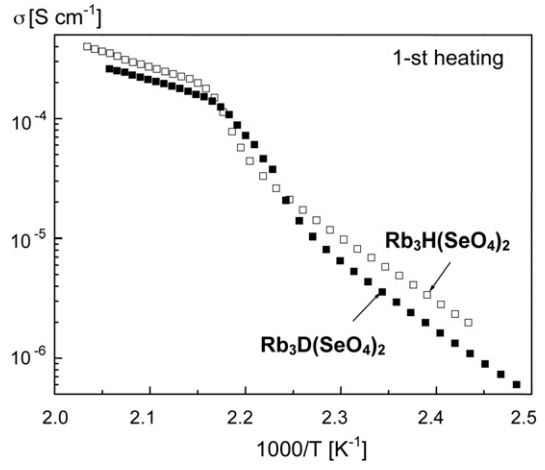

Fig. 3. Temperature variation of $H^+(D^+)$ conductivity for $Rb_3H(SeO_4)_2$ and $Rb_3D(SeO_4)_2$ in the first heating run.

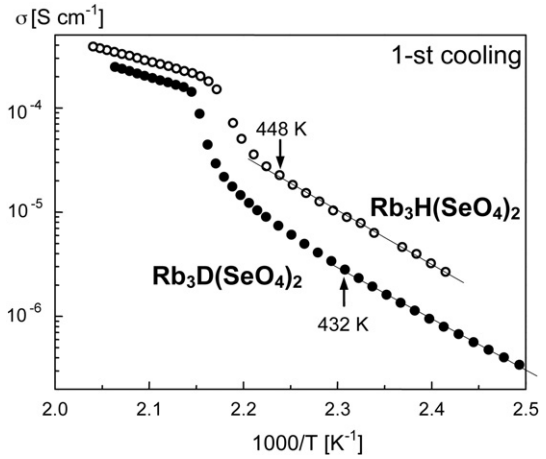

Fig. 4. Temperature variation of $H^+(D^+)$ conductivity for $Rb_3H(SeO_4)_2$ and $Rb_3D(SeO_4)_2$ in the first cooling run.

for $Rb_3D(SeO_4)_2$ crystal along the *c*-axis, differs considerably from the dependences measured in subsequent cooling/heating cycles. The distinct conductivity change at T_S, characteristic of the superionic phase transition [15], appears at a lower temperature on heating than on cooling (inverse hysteresis). The conductivity of $Rb_3D(SeO_4)_2$ in the low temperature phase is higher on the first heating than on cooling from the superionic phase. In the first heating/cooling cycle of $Rb_3D(SeO_4)_2$ the inverse thermal hysteresis of σ, i.e. the temperature difference between the parts of $\sigma(1/T)$ curves at the highest slope is more than 10 K. The hysteresis of T_S, i.e. the temperature difference between the low temperature limits of the superionic phase (on heating and cooling) is smaller and amounts to ~5 K. On the other hand, no hysteresis has been observed in the conductivity behavior of $Rb_3H(SeO_4)_2$. Figs. 3 and 4 show that there is practically no difference between the conductivity curves obtained on heating and cooling.

As shown in Fig. 4, the transition to the monoclinic phase on cooling is completed at ~450 K in $Rb_3H(SeO_4)_2$, whereas in the deuterated crystal it is completed at ~430 K. The temperatures are close to the respective DSC peaks (Figs. 1 and 2). The activation energies of ionic conductivity in the superionic phase are the same in the limit of the error: $E_c = 0.49$ eV in $Rb_3H(SeO_4)_2$ and 0.50 eV in $Rb_3D(SeO_4)_2$

3.3. Room temperature Raman spectra and X-ray study

Fig. 5 shows the NIR Raman spectra of $Rb_3H(SeO_4)_2$ and $Rb_3D(SeO_4)_2$ crystals recorded at room temperature. The spectra are very similar but it should be observed that the stretching vibrations $\mu(DSeO_4)$ appear at higher wavenumber (788.9 cm^{-1}) than the $\mu(HSeO_4)$ ones (778.6 cm^{-1}). It is obvious, that substitution of a higher mass without any change in the H-bond parameters has to result in a decrease in the donor frequency. The observed increase in the wavenumber seems to be a result of a competition between the higher mass substitution and the geometric isotope effect. To learn about the deuteration-induced changes in the H(D)-bond parameters, X-ray diffraction data of both crystals were collected at room temperature. Table 1

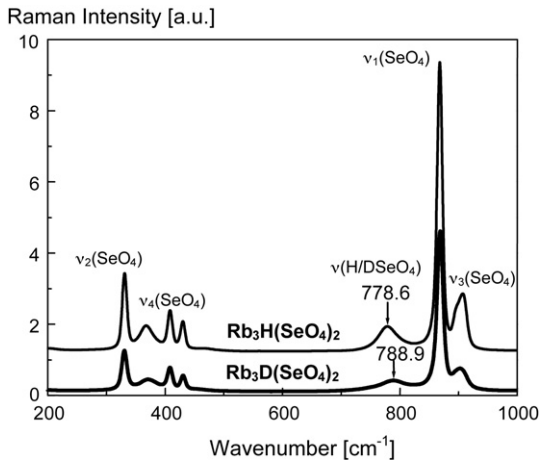

Fig. 5. Room temperature Raman spectra of $Rb_3H(SeO_4)_2$ and $Rb_3D(SeO_4)_2$ single crystals in the range of skeletal vibrations modes.

summarizes the basic crystallographic data derived at 295 K and Table 2 shows the parameters of the H/D-bond in both crystals. Apart from the difference in the O–H···O and O–D···O angles, the distance between donor O(2) atom and deuteron in $Rb_3D(SeO_4)_2$ is considerably greater than the donor O(2)–H separation in $Rb_3H(SeO_4)_2$. The increase in $\mu(DSeO_4)$ indicates therefore, that the effect of deuterium-induced changes in the geometry of the dimers prevails over that resulting from the mass increase.

3.4. Temperature evolution of the ferroelastic domain structure

The superionic transition in $Rb_3H(SeO_4)_2$ and $Rb_3D(SeO_4)_2$ is accompanied with a change in the crystal structure from the monoclinic 2/*m* to the rhombohedral $R\bar{3}m$. According to the symmetry considerations [16,17], such a transformation results in a possible appearance of three orientation states in the 2/*m* phase. The states correspond to three types of ferroelastic domains that can be separated by up to six kinds of admissible domain walls. The crystal structure is identical in each of the states, but the states differ in the spontaneous strain. The mechanical stress can transform one orientation state into another, but different states can coexist in a crystal with no applied stress since they are energetically equivalent. The crystals studied transform at T_C into the so-called prototype structure ($R\bar{3}m$), where the spontaneous strain (and also ferroelastic domain structure) vanishes.

The temperature variation of the ferroelastic domain pattern shown in Fig. 6, was observed on the (0 0 1) surface of the virgin crystals. The sample of $Rb_3D(SeO_4)_2$ was divided into two variants at room temperature (one wall separating two ferroelastic domains) and $Rb_3H(SeO_4)_2$ one had a multidomain structure with large single-domain areas. The domain pattern did not change on heating up to ~435 K in $Rb_3D(SeO_4)_2$ (~22 K below T_C) and to ~459 K in $Rb_3H(SeO_4)_2$ (~7 K below T_C). At these temperatures the thin domains of other

Table 1
Crystal data and structure refinement for $Rb_3D(SeO_4)_2$ and $Rb_3H(SeO_4)_2$

Identification code	$Rb_3D(SeO_4)_2$	$Rb_3H(SeO_4)_2$
Empirical formula	D2 O16 Rb6 Se4	H2 O16 Rb6 Se4
Formula weight	1088.69	1086.68
Temperature (K)	293(2)	293(2)
Wavelength (Å)	0.71073	0.71073
Crystal system, space group	Monoclinic, *C*2/*c*	Monoclinic, *C*2/*c*
Unit cell dimensions	$a = 15.403(3)$ Å, $\alpha = 90°$; $b = 6.0850(10)$ Å, $\beta = 102.95(3)°$; $c = 10.461(2)$ Å, $\gamma = 90°$	$a = 15.459(3)$ Å, $\alpha = 90°$; $b = 6.0910(10)$ Å, $\beta = 103.02(3)°$; $c = 10.482(2)$ Å, $\gamma = 90°$
Volume (Å^3)	955.5(3)	961.6(3)
Z, calculated density (Mg m^{-3})	2, 3.784	2, 3.753
Absorption coefficient (mm^{-1})	22.933	22.787
Crystal size	0.26 mm × 0.22 mm × 0.19 mm	0.31 mm × 0.26 mm × 0.21 mm
Theta range for data collection (°)	4.27–27.47	3.61–33.14
Reflections collected/unique	2510/591 [R(int) = 0.0673]	5498/1599 [R(int) = 0.1181]
Completeness to theta = 27.47	54.1%	86.6%
Refinement method	Full-matrix least-squares on F^2	Full-matrix least-squares on F^2
Data/restraints/parameters	591/1/65	1599/1/65
Goodness-of-fit on F^2	1.031	1.167
Final R indices [$I > 2\sigma(I)$]	$R1 = 0.0440$, w$R2 = 0.1100$	$R1 = 0.0541$, w$R2 = 0.1199$
R indices (all data)	$R1 = 0.0489$, w$R2 = 0.1136$	$R1 = 0.0711$, w$R2 = 0.1255$
Extinction coefficient	0.00385(9)	0.00235(7)

Table 2
Details of hydrogen bonds (Å, °) at 295 K (D—donor, A—acceptor, D(1)—deuterium)

Compound	D–H	*d*(D–H)	*d*(H···A)	∠DHA	*d*(D···A)	A
$Rb_3D(SeO_4)_2$	O(2)–D(1)	0.949	1.621	167.72	2.556	O(2) [$-x+1, -y, -z$]
$Rb_3H(SeO_4)_2$	O(2)–H(1)	0.912	1.676	159.01	2.548	O(2) [$-x+1, -y, -z$]

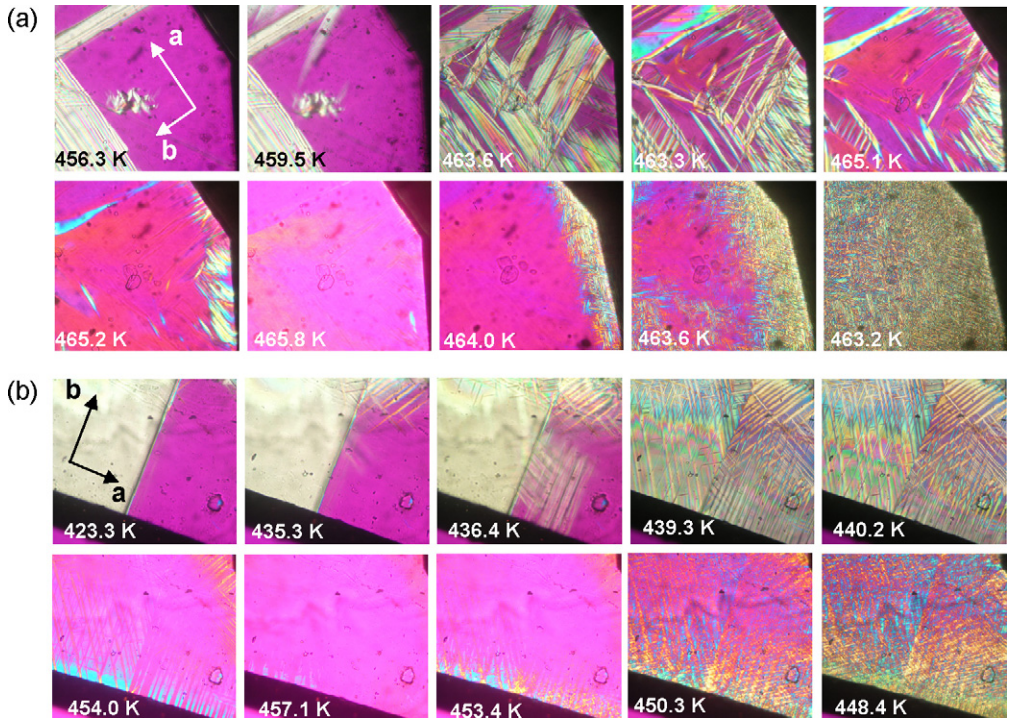

Fig. 6. Temperature evolution of ferroelastic domain structure in a) $Rb_3H(SeO_4)_2$ and b) $Rb_3D(SeO_4)_2$.

orientation states started to appear and their number increased on further heating. The changes in the microscope image, which we interpreted as the appearance of nuclei of the high temperature phase, started at ~450 K in $Rb_3D(SeO_4)_2$ (~7 K below T_C) and ~464 K in $Rb_3H(SeO_4)_2$ (~1 K below T_C). At their respective T_C, the crystals transformed to the paraelastic (superionic) phase and the ferroelastic domains disappeared.

4. Discussion

The data published so far show slight differences in the temperature behavior of $Rb_3H(SeO_4)_2$ crystal. For instance the difference in T_S value, which was reported to range from 449 K to 456 K [3,7–9] can be related, in our opinion, to different concentrations of lattice defects in the crystals grown in slightly different conditions. Also the number, shape and separation of peaks of DSC anomaly in the superionic transition region [9,18], as well as the details of the physical behavior in the so-called "intermediate phase" (temperature evolution of ferroelastic domain structure, symmetry change) [9,19] may depend on the conditions in which a given crystal was grown.

Irrespective of the above differences, the proton conductivity value and the anisotropy of the activation energy in the superionic phase are very similar for various $Rb_3H(SeO_4)_2$ crystals [15,20]. In the present work we obtained the activation energy along the c-axis as $E_c^H = 0.49$ eV for $Rb_3H(SeO_4)_2$ above T_S, which agrees with earlier results.

For $Rb_3D(SeO_4)_2$, the activation energy was $E_c^D = 0.50$ eV in the high temperature phase, which contrasts with $E_c = 0.28$ eV reported in [10]. We consider $E_c^D = 0.50$ eV to be a reasonable value, since the same molecular mechanism is responsible for the ionic conductivity in $Rb_3H(SeO_4)_2$ and $Rb_3D(SeO_4)_2$. Furthermore, both crystals undergo the same change of symmetry at T_S and show similar properties (ferroelastic, superionic). In the superionic phase of hydrogen sulfates and selenates the high dynamics of XO_4 tetrahedra results in fluctuations of O(2) oxygen atoms (donor and acceptor) separation. The fluctuations are large enough for proton (deuteron) transfer from donor to acceptor in its vibrational ground state, so the potential barrier for deuteron transfer is expected to be a little higher (by the energy difference of H^+ and D^+ ground states) [4]. A possible reason for the discrepancy may be the one-frequency method of the conductivity measurement in [10].

As mentioned, the huge H/D isotope effect in $Rb_3H(SeO_4)_2$ was found in the low temperature range (deuteration-induced antiferroelectric phase transition) [12]. On the other hand, we observed a rather small difference in the T_S value ($T_S^H - T_S^D \approx 5$ K) between protonated and deuterated crystals on the first heating. The conductivity ratio between $Rb_3H(SeO_4)_2$ and $Rb_3D(SeO_4)_2$ was approximately 1.6, which points to a classical activated diffusion mechanism [13,21].

Qualitatively similar high temperature behavior was reported for another superionic acid salt, $CsHSO_4$ [13,14,22]. The very small isotope effect on the superionic proton conductivity in $Rb_3H(SeO_4)_2$ shows that protons (deuterons) follow the dynamics of their environment without encountering considerable barriers along the diffusion path and substitution protons by deuterons does not significantly influence the intensive dynamics of the selenate tetrahedra.

Polarization microscope observation of the temperature evolution of the ferroelastic domain pattern, as well as DSC and $\sigma(T)$ measurements indicate, that the temperature range of superionic phase transition differs in the two crystals studied. On the other hand, the transition in both crystals is accompanied with structural reconstruction of the lattice from $C2/c$ to $R\bar{3}m$ and with a great increase in the molecular dynamics. Indeed, the transition enthalpy is similar in the two crystals, so one can infer that similar energy consuming processes are involved. Our results indicate that the processes in $Rb_3D(SeO_4)_2$ are spread over a much wider range of temperatures.

The temperature evolution of the ferroelastic domain structure (Fig. 6) shows that in a virgin crystal new domains start to appear in $Rb_3D(SeO_4)_2$ on the first heating at $T_C - T \approx 22$ K and in $Rb_3H(SeO_4)_2$ at $T_C - T \approx 7$ K. Similarly, the high temperature phase nuclei in $Rb_3D(SeO_4)_2$ start to grow ~7 K, whereas in $Rb_3H(SeO_4)_2$ only at ~1 K below T_C. The energy of a domain wall (i.e. the energy of formation of a twin) decreases with increasing temperature and disappears at T_C, at which no energy is required to form a twin wall. The increasing ease with which domain walls can be formed on heating is equivalent to the well-known effect of an elastic softening of the crystal structure on approaching T_C [23]. The number of walls in a crystal depends exponentially on their formation energy. As a result a dense domain pattern is observed in both crystals close to T_C (Fig. 6). The formation of new twins at greater $(T_C - T)$ distance in $Rb_3D(SeO_4)_2$ points to a more elastically "soft" structure of the deuterated crystal.

It is worth noting, that there is a correlation between the ferroelastic domain evolution in the two crystals and their respective thermal anomalies: the domain pattern starts to change on the first heating at a temperature, which is close to the position of the respective DSC peak. The temperatures at which the nuclei of the high temperature phase start to appear (~450 K in $Rb_3D(SeO_4)_2$ and ~464 K in $Rb_3H(SeO_4)_2$) are close to those at which the highest slope of σ $(1/T)$ is observed. Similarly, the temperatures T_C at which the ferroelastic domain structure vanishes (~457 K and ~465 K) are near to the respective T_S values, which set the low temperature limits of the superionic phase (with $E_c \approx 0.50$ eV) on the σ $(1/T)$ dependence.

5. Conclusions

DSC, ionic conductivity and ferroelastic domain structure studies of the isotope effect on the superionic phase transition in $Rb_3H(SeO_4)_2$ single crystal have shown that deuteration (to a degree of approximately 90%) results in a downward shift of the transition temperature in the first heating run, but practically does not affect the activation energy value ($E_c \approx 0.50$ eV) in the superionic phase. The small H/D isotope effect on the proton conductivity is comparable with that reported for $CsHSO_4$ and points to a classical activated diffusion mechanism: proton (deuteron) follows the dynamics of its neighborhood and the dynamics does not change significantly on substitution of protons by deuterons. It has been found that the temperature variation of the ionic conductivity in $Rb_3D(SeO_4)_2$ differs considerably in the first heating run from that obtained on cooling and in subsequent heating–cooling cycles. Such behavior was not observed in the non-deuterated crystal. Furthermore, the ionic conductivity study of $Rb_3D(SeO_4)_2$ has revealed an inverse thermal hysteresis of T_S, whereas the protonated crystal has not exhibited any hysteresis.

The difference in the temperature evolution of the ferroelastic domain pattern in $Rb_3D(SeO_4)_2$ and $Rb_3H(SeO_4)_2$ single crystals corresponds to the results of DSC and impedance spectroscopy studies and points to a more diffuse character of the superionic phase transition in $Rb_3D(SeO_4)_2$. The temperature range of the transition in $Rb_3D(SeO_4)_2$ is stretched over 18–22 K, whereas in $Rb_3H(SeO_4)_2$ crystals this range amounts only to ~7 K. The room temperature ferroelastic domain pattern remains static on the first heating up to $T_C - T \approx 22$ K in $Rb_3D(SeO_4)_2$ and $T_C - T \approx 7$ K in $Rb_3H(SeO_4)_2$. At these temperatures new domain walls start to grow. The greater ease of formation of the walls in $Rb_3D(SeO_4)_2$ indicates that the crystal structure is elastically softer compared with that of $Rb_3H(SeO_4)_2$.

The room temperature NIR Raman spectra of the skeletal modes in $Rb_3D(SeO_4)_2$ and $Rb_3H(SeO_4)_2$ crystals point to a competition between the conventional isotope effect (i.e. decrease in the wave number) and deuterium-induced geometric changes in the $O_3SeO(2)$–$H(D)\cdots O(2)SeO_3$ dimers.

Acknowledgment

The work was supported by Grant 1 P03B 030 28 from the Committee of Scientific Research in Poland.

References

[1] S.M. Haile, D.A. Boysen, C.R.I. Chisholm, R.B. Merle, Nature 410 (2001) 910.
[2] R.B. Merle, C.R.I. Chisholm, D.A. Boysen, S.M. Haile, Energy Fuels 17 (2003) 210.
[3] A.I. Baranov, I.P. Makarova, L.A. Muradyan, A.V. Tregubchenko, L.A. Shuvalov, Sov. Phys. Crystallogr. 32 (1987) 400.
[4] K.D. Kreuer, Chem. Mater. 8 (1996) 610.
[5] A. Pawłowski, B. Hilczer, Oxide-ion and protonic solid electrolytes, in: C. Boulesteix (Ed.), Oxides, Key Engineering Materials, Trans Tech Publications, Zurich, 1998, pp. 155–156.
[6] A. Pawłowski, M. Połomska, Solid State Ionics 176 (2005) 2045.
[7] A. Pawłowski, C. Pawlaczyk, B. Hilczer, Solid State Ionics 44 (1990) 17.
[8] M. Ichikawa, J. Phys. Soc. Jpn. 47 (1979) 681.
[9] A. Pawłowski, L. Szcześniak, M. Połomska, B. Hilczer, L. Kirpichnikova, Solid State Ionics 157 (2003) 203.
[10] Y. Matsumoto, J. Phys. Soc. Jpn. 70 (2001) 155.
[11] T. Gustafsson, M. Ichikawa, I. Olovsson, J. Kor. Phys. Soc. 32 (1998) S199.
[12] M. Ichikawa, K. Motida, T. Gustafsson, I. Olovsson, Solid State Commun. 76 (1990) 547.
[13] V.V. Sinitsin, E.G. Ponyatovskii, A.I. Baranov, A.V. Tregubchenko, L.A. Shuvalov, JETP 100 (1991) 693 (in Russian).
[14] T. Norby, M. Friesel, B.E. Mellander, Solid State Ionics 77 (1995) 105.
[15] A. Pawłowski, C. Pawlaczyk, Ferroelectrics 81 (1988) 201.

[16] W. Schranz, P. Dolinar, A. Fuith, H. Warhanek, Phase Transit. 34 (1991) 189.
[17] J. Sapriel, Phys. Rev. B 12 (1975) 5128.
[18] R.A. Dilanyan, V.V. Sinitsyn, V.Sh. Shekhtman, A.I. Baranov, L.A. Shuvalov, Kristallografia 39 (1994) 484 (in Russian).
[19] B.V. Merinov, S.M. Haile, V. Bismayer, Solid State Ionics 146 (2002) 355.
[20] A.I. Baranov, Kristallografia 48 (2003) 1081.
[21] A.S. Nowick, A.V. Vaysleyb, Solid State Ionics 97 (1997) 17.
[22] Th. Dippel, N. Hainovsky, K.D. Kreuer, W. Münch, J. Maier, Ferroelectrics 167 (1995) 59.
[23] E.K.H. Salje, Phase Transitions in Ferroelastic and Co-elastic Crystals, Cambridge University Press, Cambridge, 1990.